Connectopic mapping of the dorsal and ventral visual processing pathways using task-based fMRI.

A THESIS

submitted in partial fulfilment of the requirements

for the award of the dual degree of

Bachelor of Science - Master of Science

in

BIOLOGICAL SCIENCES

by

YUDHAJIT AIN

(16231)

DEPARTMENT OF BIOLOGICAL SCIENCES

INDIAN INSTITUTE OF SCIENCE EDUCATION AND

RESEARCH BHOPAL

BHOPAL – 462 066

May 2021

भारतीय विज्ञान शिक्षा एवं अनुसंधान संस्थान भोपाल
Indian Institute of Science Education and Research Bhopal
(Estb. by Ministry of HRD, Govt. of India)

CERTIFICATE

This is to certify that Yudhajit Ain, BS-MS (Dual Degree) student in the Department of Biological Sciences, has completed bonafide work on the thesis entitled '**Connectopic mapping of the dorsal and ventral visual processing pathways using task-based fMRI.**' under my supervision and guidance.

May 2021   Dr. Nagarjun Vijay

IISER Bhopal   (supervisor)

May 2021   Dr. Arpan Banerjee

NBRC Manesar   (co-supervisor)

Committee Member	Signature	Date
Dr. Nagarjun Vijay		19th May2021
Dr. Sourav Datta		
Dr. Ajit Chande		

ACADEMIC INTEGRITY AND

COPYRIGHT DISCLAIMER

I hereby declare that this project report is my own work and due acknowledgement has been made wherever the work described is based on the findings of other investigators. This report has not been accepted for the award of any other degree or diploma at IISER Bhopal or any other educational institution. I also declare that I have adhered to all principles of academic honesty and integrity and have not misrepresented or fabricated or falsified any idea/data/fact/source in my submission.

May 2021
IISER Bhopal

Yudhajit Ain

ACKNOWLEDGEMENT

Yudhajit Ain

ABSTRACT

Progress in resting-state fMRI analysis now allows us to explore even how the topographic functional connectivity between different brain areas varies with time. Perhaps the most challenging part of the exploration of connectivity topographies (connectopies) is to hypothesise and explain the functional importance of such connectopies, and what their structures imply for information flow and computation within the neuronal network. Here we build upon our previous elucidation of the canonical visual pathways and provide further arguments for the complex interdependence between the posited dorsal and ventral visual pathways. We look at how learning of a task-paradigm leads to changes in integration and segregation between the pathways with the help of connectopic mapping between them.

LIST OF ABBREVIATIONS

Abbreviation	Extended form
ROI(s)	Region(s)-of-interest
VOI(s)	Voxel(s)-of-interest
SPM	Statistical Parametric Mapping
SD	Standard deviation
TR	Repetition Time
TE	Echo Time
BA	Brodmann Area
ANOVA	Analysis of Variance
SPSS	Statistical Package for the Social Sciences

LIST OF FIGURES

LIST OF TABLES

CONTENTS

Introduction

Topography in connectivity refers to the spatial organisation of connectivity between brain areas. This can be of any kind, for example, point-to-point mappings such that nearby voxels in one region connect to nearby voxels in the other region, or connections that break topology and make clusters in the target area[1].

Topographic maps are very common in the human brain. Most sensory neuronal fields (like the retina) preserve their topographical organisation, through a number of relay nuclei, right up to the cortex. For example, retinofugal projections are retinotopically organised, projections to the cochlear nucleus are tonotopically organised, and projections from the skin to the primary sensory cortex are somatotopically organised. Topographies are also found in cortico-cortical, cortico-subcortical and cortical-cerebellar connections.

An interesting observation is that multiple overlapping topographical maps may characterise the same brain area depending on the target region under consideration. So while region A may connect to region B in a topology-preserving point-to-point fashion, it may also connect to a region C such that fibres from A make two or more clusters in region C. Hence, the projections from region A are topographically organised separately in two different dimensions.

The most convenient method to uncover a topographical map is to gradually vary a continuous variable (e.g. position of visual stimulus) and look for corresponding continuous changes in the position of regions of activation in the brain. Recent advances in neuroimaging analysis have however made it possible to look for topographic maps even in the absence of an externally varied stimulus (or continuous variable). The principle is essentially simple- the experimenter can consider a seed region of interest within the brain, and using an appropriate measure of brain connectivity, monitor for a gradual change in the position of the target region(s) as the position of the seed region is continuously varied. This method has been used by many groups to uncover topographic connections *without a task,* for example Heinzle et al. using resting fMRI[2], and another group[3] using

diffusion-fMRI (dfMRI), a method that relates to structural connectivity by tracking the diffusion of water through white matter fibres.

The more challenging part of research in topographical brain connectivity is to rationalise the importance of and the need for the existence of such connectivity in the first place. While it makes sense that topographic connectivity is an efficient method of performing local computations with respect to early relay nuclei and primary sensory cortices by grouping together neurons that interact the most (and are adjacent in their receptive fields), there are varied opinions regarding their functions in higher-order cortico-cortical connections. It has been suggested that cortico-cortical connectopies encode more abstract representations to facilitate simple instances of learning, logic and reasoning [4].

Perhaps the most unified hypothesis that explains the structure of cognition with respect to the topographical organisation of the cortex is as follows. Neuroscientists propose the "principle of superposition" of connection patterns (or modes) across hierarchically arranged gradients of topography across the cortex in such a manner that loading of inputs into the region of interest from either extreme of the gradient either tips the balance of neural computation depending on the task's demand. For example, a cortical region that receives topographical inputs from sensory projections, as well as top-down projections, can effectively give rise to simple mechanisms for coincidence detection[5], which can then be biased towards either rapid, low-level perception or focused, attentive analysis depending on whether the former or latter source of input is weighted more strongly.

Using large-scale topographic analysis to model cognition is still new, and little work has been done to explore the implications of changes in connectopy on information processing. Hence, our primary objective was to explore the effect of learning on the local topographic connectivity between the canonical dorsal and ventral visual pathways. Moreover, we aimed at refining the Mishkin-Ungerleider[6] and Milner-Goodale[7] models of visual information processing by reviewing the task-based fMRI connectivity between the visual pathways through the lens of this new gradient-based approach.

Materials and methods

MRI data acquisition and experimental design

All fMRI data was acquired at National Brain Research Centre, India and reported previously by Ray et al. 2020 [8]. 20 human participants (mean age = 25.35 years, SD = 2.796 years, 11 females) participated in the study by signing informed consents, which along with the study protocol was approved by the Institutional Human Ethics Committee of NBRC. My analysis used de-identifiable data that was published in Ray et al 2020 and never during the analysis was any attempt made to violate their privacy. Structural images (T1-weighted) were obtained with repetition time (TR) = 8.4 ms, echo time (TE) = 3.7 ms, flip angle = 8 degree, matrix = 252 x 230 x 170 mm (Fig. 1A). Functional images (T2*-weighted) were obtained with TR = 2000 ms, TE = 35 ms, flip angle = 90 degree, matrix = 60 x 62 x 30 using a gradient EPI sequence (Fig. 1B).
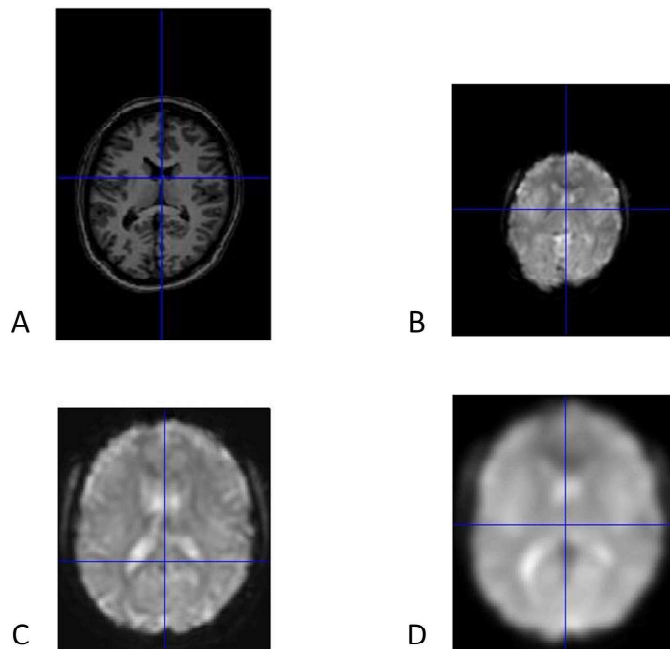
Figure 1. (A) Structural (T1-weighted) image, **(B)** Functional motion-corrected T2*-weighted image, **(C)** Functional image normalised to the MNI template, and **(D)** Normalised functional image after smoothing of the same coronal slice of one representative subject.

A block-design was used for the experiment and two types of responses (*perception task* and *visually guided action task*) and three types of stimuli (*colour*, *face* and *position*) were used. In all perception tasks, the subjects had to report how many times the target stimulus (informed before the start of the trial) appeared. For the action tasks, the response variable was the reaction time (RT) required by the subject to move a cursor (using a joystick) to the target. The experimental paradigm has been outlined schematically in Fig. 2.
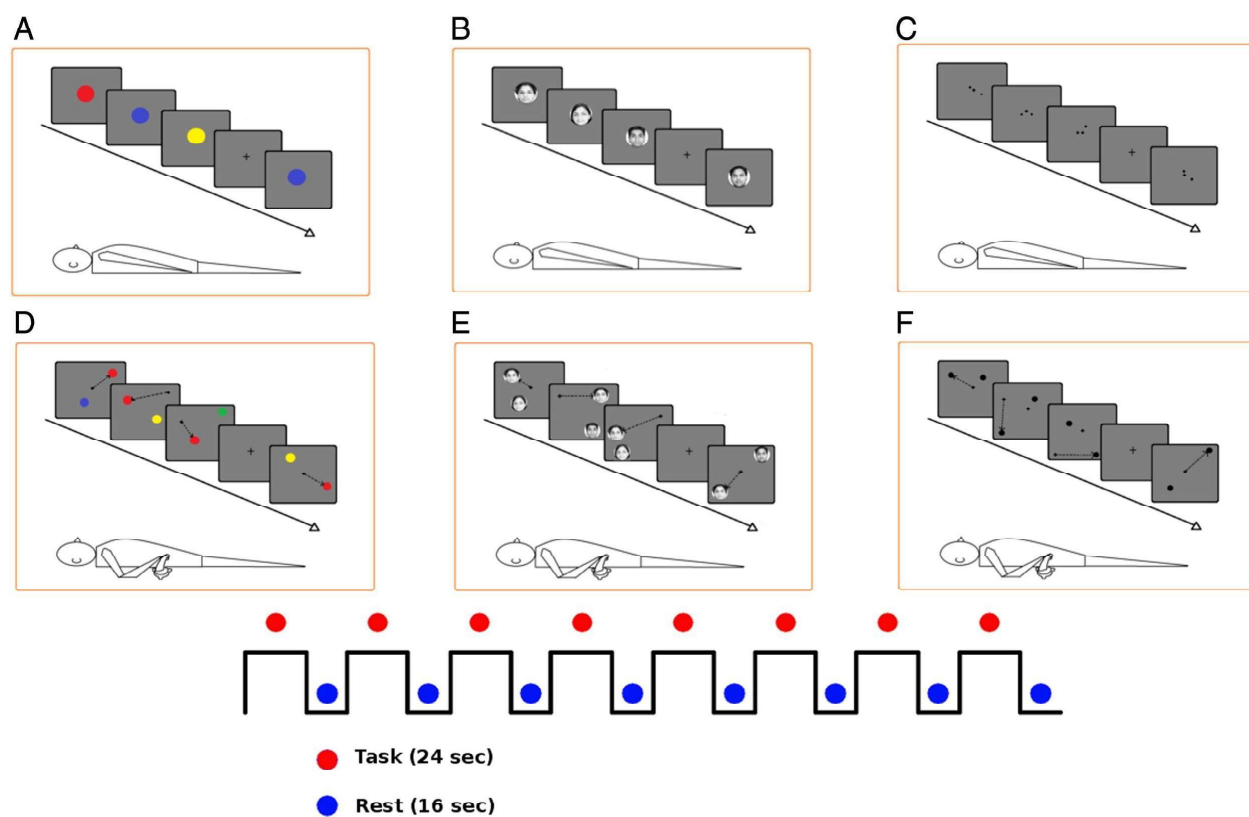
Fig. 2. **(A), (B), (C)** - *perception tasks*. **(D), (E), (F)** - *action tasks*. The trial duration was 1 s for the perception tasks and the time to move the cursor to the target, or a maximum of 4 s (whichever is smaller) in the action tasks. Stimulus and task order were randomised for each participant and task and rest blocks of 24 s and 16 s respectively were alternated in each run. Figure adapted from Ray et al. BioRx 2018 under a Creative Commons License of reproduction for academic purposes.

MRI data preprocessing and ROI definition

Preprocessing of the fMRI data was carried out using SPM12 toolbox (www.fil.ion.ucl.ac.uk/spm/). To get rid of transient artefacts due to unstable magnetisation, we discarded an initial epoch of the first 8 s. The T2*-weighted images were slice-time corrected, motion-corrected and realigned with the mean T2* image, followed by coregistration with the corresponding T1 image, normalisation to the Montreal Neurological Institute (MNI) template and resampling to 3.5 mm isotropic voxel dimensions (Fig. 1C). Finally, the signals were also smoothed using a Gaussian kernel of 8 x 8 x 10 mm^3 FWHM (full-width-at-half-maximum). All the smoothed images (Fig. 1D) consequently obtained from a single run were concatenated to obtain the smoothed 4-dimensional NIFTI time-series files used for further analysis. Second-degree and fourth-degree B-spline interpolation was employed for the estimation and reslicing steps respectively during motion-correction. For coregistration, the mutual information objective function was maximised, and for normalisation, fourth-degree B-spline interpolation was used.

In line with the goal of teasing apart the connectopic structure of the visual processing system, a combined ROI mask (Fig. 3) was defined, which included components of the canonical ventral stream (ventral extrastriate cortex, fusiform gyrus and the lateral occipital cortex), the canonical dorsal stream (dorsal extrastriate cortex, superior parietal cortex, intraparietal sulcus, inferior parietal cortex, and V5/MT+), and the V1/V2 region (BA 17 and BA 18). We used the SPM Anatomy toolbox to create the probabilistic cytoarchitectonic mask.
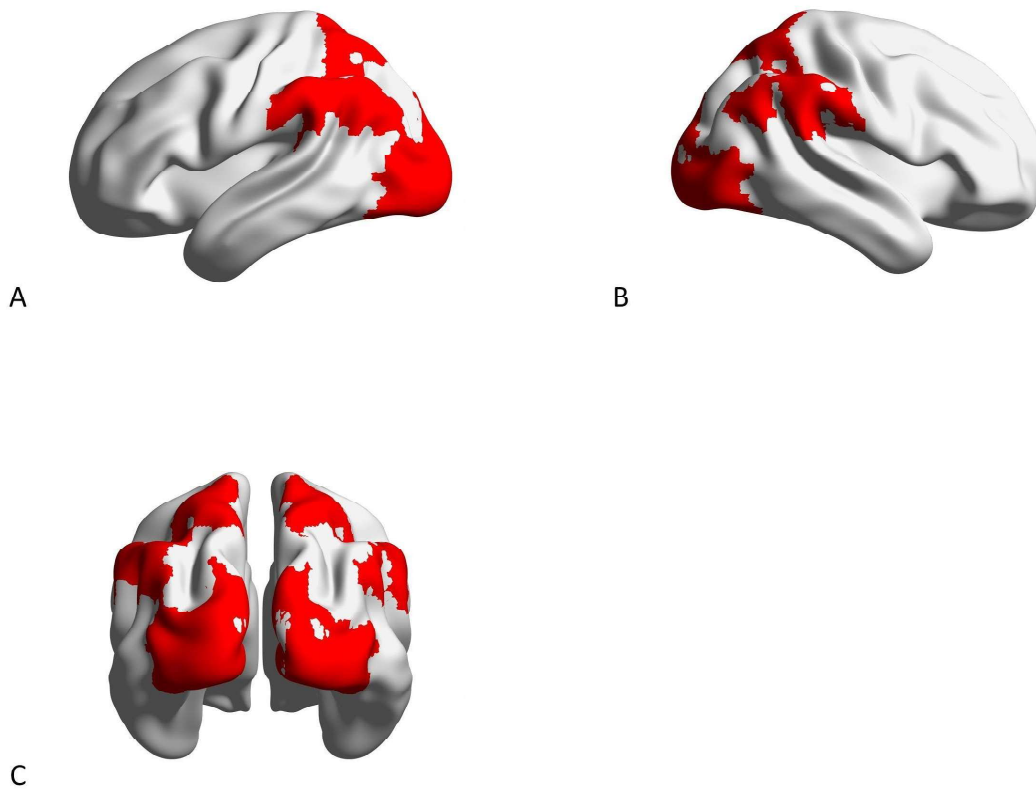
Figure 3. (A) Left, **(B)** right, and **(C)** caudal view of the region of interest (visual processing system) obtained using BrainNet Viewer. The ROI has been mapped on the smoothed ICBM MNI152 template brain. Figure generated in BrainNet Viewer.

Connectopic mapping

There are several problems associated with the aforementioned "moving-seed" method for discovering connectopic organisation from fMRI data. Firstly, if the region-of-interest has multiple overlapping connectopies, that is, more than one mode of topographic connectivity (like retinotopy in the V1 region) it will uncover the superposition of all of them instead of the multiple separate underlying connectopic gradients. Secondly, a topographic organisation emerges after carefully looking at and identifying gradual changes in the target location as one moves the seed in a particular manner. However, there are practically infinite ways

of moving across a cortical ROI, and a completely exhaustive exploration of all of them is impractical and barely feasible.

This problem has been overcome by using a completely data-driven approach of uncovering the principal functional connectivity topographies across the ROI from the task-fMRI time-series of each subject under each scanning condition. The pipeline, established by Haak et al[9] consists of two intuitively appealing steps:

(a) Connectivity fingerprinting - first, we identify p *(= t-1)* temporally uncorrelated spatial independent components (sICs) within the rest of the brain (excluding the ROI), where t is the number of rows, or time points, in the matrices **A** and **B**. The number of columns in **A** and **B** is the number of voxels within the ROI and the rest of the brain respectively. Using singular value decomposition (SVD) to dimension-reduce **B** to **B`** makes the algorithm more computationally tractable. If **B = UΣV\*,** then **B` = U`Σ`** where **Σ`** is the $p$ x $p$ reduced-rank singular-value matrix containing the $p$ largest singular values, and **U`** is the corresponding truncated **U** matrix. The column vectors of **B`** are therefore the time-series of the BOLD signal along individual spatial modes. p of these spatial modes are considered. It must be noted that p is generally large enough to explain around 100 percent of the variance in **B**, such that this does not result in a loss of much reliable signal.

The connectivity fingerprints of all the voxels in the ROI (corresponding to all the columns of **A**) are then obtained by finding out the Pearson's correlation between the time-series of that voxel, and each of the time-series along the columns of **B`** respectively. This, therefore, gives us one row per ROI-voxel within the matrix **C,** along whose $p$ columns we have the functional connectivity of said ROI-voxel with the $p^{th}$ spatial component in **B`**.

(b) Non-linear manifold learning - The matrix **C** can be treated as a data matrix where each row is a p-dimensional data point, whose projection along each basis vector is the functional connectivity of said VOI with that specific spatial component represented by that basis vector. The interesting idea is that because of the topography of the ROI, voxels nearby in the anatomical space map close together in the p-dimensional space. Thus, the assumption is that the data points in

our p-dimensional space intrinsically lie along a lower-dimensional manifold. As mentioned before, this intrinsic sparsity of dimensions required to adequately represent the connectivity profiles of the voxels-of-interest (VOIs) is driven by topographic clustering. The goal of the pipeline is to learn, from empirical data itself, the nature of this lower-dimensional manifold, as well as to ensure topographic mapping through spectral embedding. That is, we try to learn a lower-dimensional mapping of the data points such that the distance between individual data points in the lower-dimensional space represents the geodesic distance between said points as measured along the manifold.

For example, Fig. 4 illustrates what manifold-learning does, using a toy-dataset. The 3-dimensional scatterplot (panel 1) is a representation of points in a higher-dimensional space (3D), which lie along an intrinsically lower-dimensional manifold (2D). Non-linear manifold learning basically makes a graph by connecting data points close to each other using edges (panel 2). Finally, using any non-linear "unrolling" algorithm, in our case by finding the eigenvectors of the graph-laplacian, the 2D manifold is obtained (panel 3). The two-basis vectors of this lower-dimensional manifold explain the variance in the dataset almost completely.
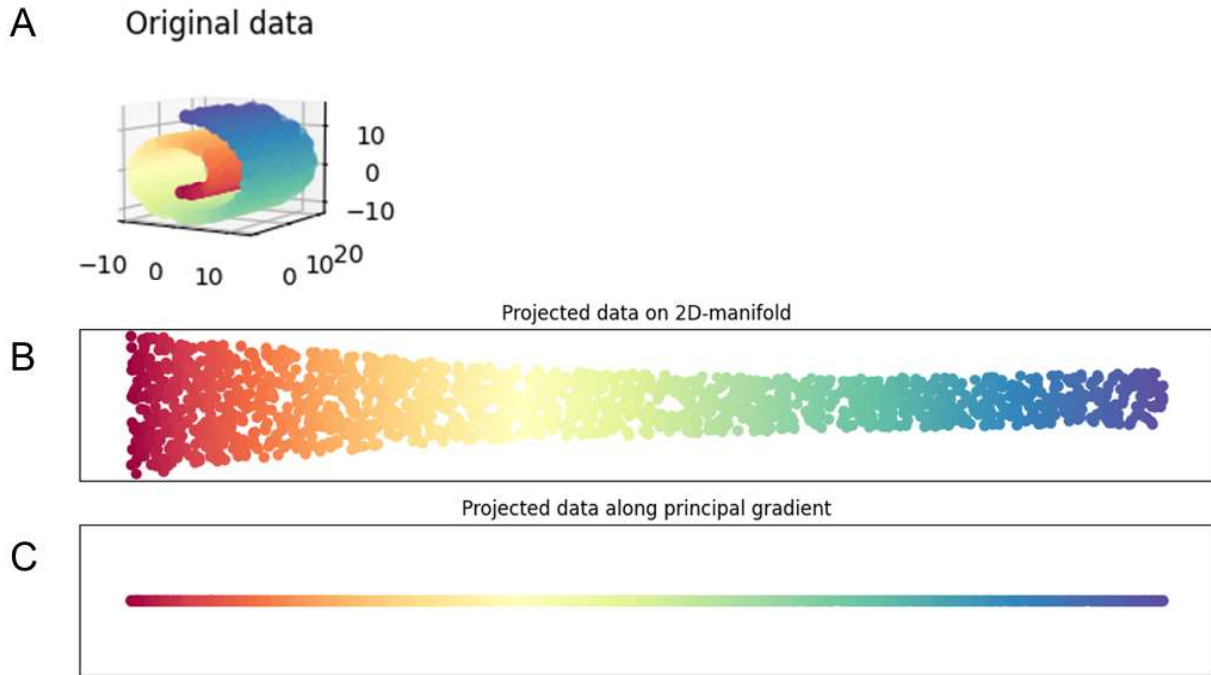
Figure 4. Illustration of the non-linear manifold-learning algorithm for a dataset where N=1800. **(A)** 3D swiss-roll. **(B)** Embedded data points on the 2D-manifold learnt by the non-linear manifold learning algorithm (here, Locally Linear Embedding). **(C)** Data points embedded along the principal basis of the 2D-manifold. Figure generated using Python.

To achieve spectral embedding of the data points in our case, a similarity matrix **S** is constructed, using the η^2 coefficient as outlined by Cohen et al.[10] The η^2 value in the αth row and the βth column of **S** gives the percentage of variance in the connectivity fingerprint of the αth VOI that is explained, or accounted for by the variance in the connectivity fingerprint of the βth VOI. The values in **S** range from 0 (completely similar connectivity fingerprints) to 1 (completely dissimilar connectivity fingerprints).

$$S_{\alpha,\beta} \quad = \quad \text{eta}^2 = 1 - \frac{SS_{\text{Within}}}{SS_{\text{Total}}} = 1 - \frac{\sum_{i=1}^{n}\left[(a_i - m_i)^2 + (b_i - m_i)^2\right]}{\sum_{i=1}^{n}\left[(a_i - \overline{M})^2 + (b_i - \overline{M})^2\right]} \qquad \textbf{(Eqn. 1)}$$

Where $a_i = \mathbf{C}_{\alpha,i}$, $b_i = \mathbf{C}_{\beta,i}$, $m_i = (a_i + b_i)/2$, and M = mean of m_i across all n (= p here). Finally, the similarity matrix is thresholded, such that we obtain one complete connected graph. The edges between VOIs are weighed, in order to do this, using

$$\mathbf{W}_{i,j} = \begin{cases} \mathbf{S}_{i,j} & \text{if } \|\mathbf{S}_{i\cdot} - \mathbf{S}_{j\cdot}\|^2 < \varepsilon \\ 0 & \text{if } \|\mathbf{S}_{i\cdot} - \mathbf{S}_{j\cdot}\|^2 \geq \varepsilon \end{cases} \qquad \textbf{(Eqn. 2)}$$

The degree matrix $\mathbf{D}$ is constructed as the diagonal matrix, with $\mathbf{D}_{i,i} = \sum \mathbf{W}_i$ whose diagonal elements represent the sum of edge-weights associated with each node (VOI). Finally, the graph Laplacian $\mathbf{L}$ is given by $\mathbf{L=D-W}$. The eigenvalues $\lambda_0 = 0 \leq \lambda_1 \leq \cdots \leq \lambda_k$ and eigenvectors $\{\mathbf{y_o}, \mathbf{y_1}, \dots, \mathbf{y_k}\}$ of $\mathbf{L}$ are given by the solutions of the generalized eigenvalue problem $\mathbf{Ly} = \lambda \mathbf{Dy}$.

The eigenvectors $\{\mathbf{y_1}, \dots, \mathbf{y_k}\}$ corresponding to the smallest k non-zero eigenvalues (the eigenvector corresponding to the zero eigenvalue trivially maps all VOIs to the same point) $\{\lambda_1, \dots, \lambda_k\}$ minimise the objective function $\sum_{i,j} [\mathbf{y(i)} - \mathbf{y(j)}]^2 \mathbf{W}_{i,j}$. That is, the eigenvectors provide us with a lower-dimensional embedding of our data points, such that VOIs with similar connectivity fingerprints are mapped closer along the k connectopies. It must be noted that the minimization basically reduces the geodesic distance (on the m-dimensional manifold) between pairs of nodes such that the geodesic distance is minimum for node-pairs with the highest edge-weights, i.e., the highest similarity between their connectivity profiles. The values in $\mathbf{y}$ are normalized to have a value between zero to one. Figure 5 outlines the pipeline schematically.
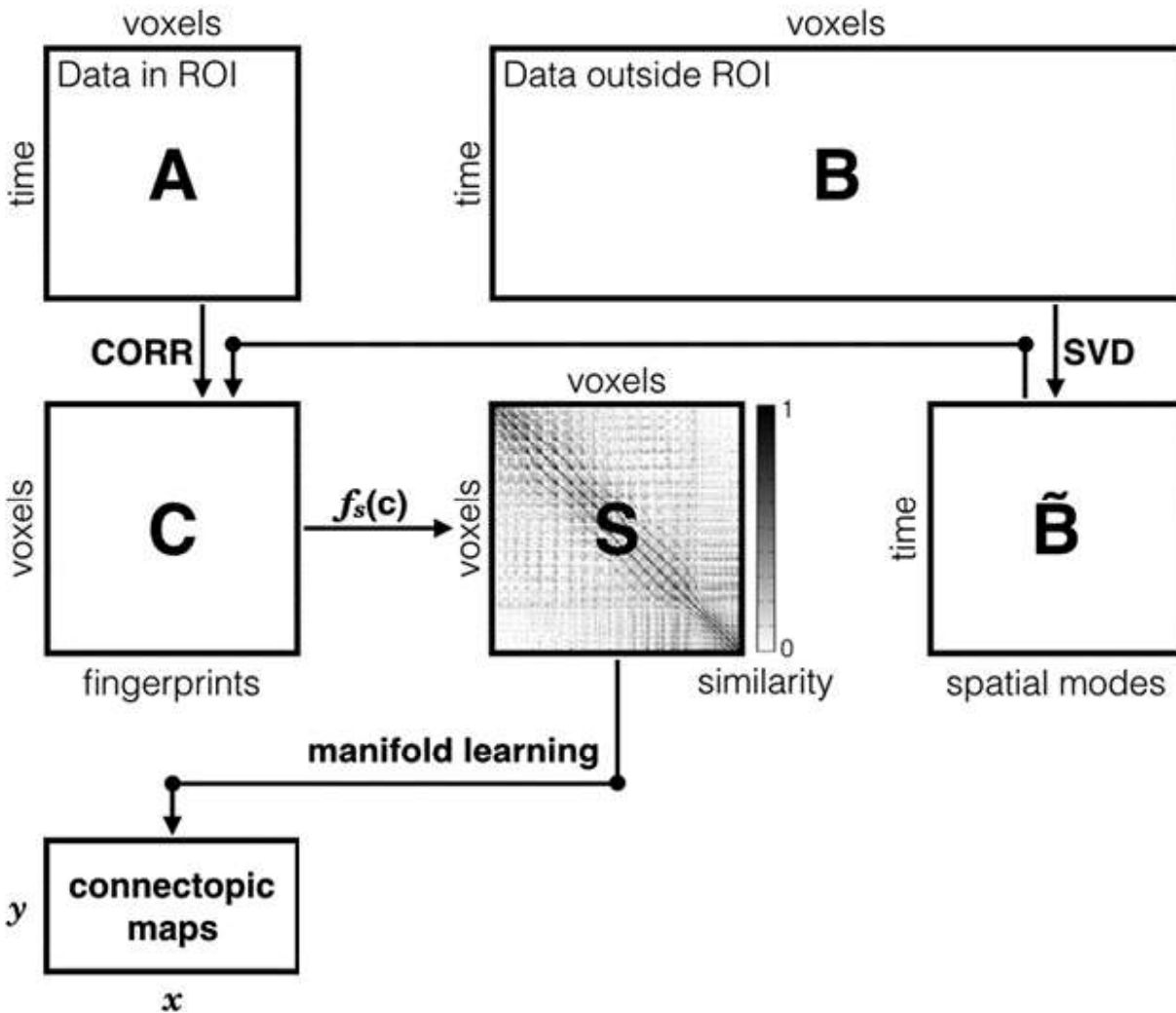
Figure 5. A schematic outline of the connectopic gradient mapping pipeline. Matrix A contains the fMRI time-series of all voxels within the ROI (here, the visual processing system), and matrix B contains the fMRI time-series of all voxels outside the ROI included within the mask. Singular Value Decomposition (SVD), a non-linear analogue of Principal Component Analysis (PCA) is used to identify only the independent eigen-components in B and lower the dimensionality of B, creating the matrix B̃. The correlation coefficient of time-series of each voxel in A with each component in B̃ is used to construct the matrix C which essentially represents the connectivity fingerprints of all voxels in A. Figure adapted from Haak et al. [9]

Results

To figure out if the factors *learning* (with levels before and after) and *task-condition* (with levels CP, CR, PP, PR, FP and FR) have any systematic effect on the gradient values of the VOIs, we performed a repeated-measures mixed-effects ANOVA, where the repeated-measure factors (within-subjects factors) were learning and task-condition, and the VOIs were grouped into three *ROIs* (Ventral stream, V1/V2 and Dorsal stream). Therefore, *ROI* is the between-subjects factor here. We used IBM SPSS for the ANOVA and subsequent posthoc multiple comparisons.

We found that assumption of sphericity is violated, i.e., Mauchly's test of sphericity was significant, for both the within-subjects factor **task** ($\chi^2(14) = 22081.854$, p < 0.001) the and the interaction **learning*task** ($\chi^2(14) = 18204.728$, p < 0.001). Thus, the degrees of freedom were corrected for the two factors using Greenhouse-Geisser estimates of sphericity: $\varepsilon=0.417$ and $\varepsilon=0.326$ respectively (Table 1).

Table. 1 Mauchly's test of sphericity

Within-subjects effect	Mauchly's W	Approx. Chi-square	df	Sig.	Epsilon (Greenhouse-Geisser)
LEARNING	1	0	0	.	1.000
TASK	.009	22081.854	14	.000	0.417
LEARNING*TASK	.021	18204.728	14	.000	0.326

We observed a significant main effect of the between-subjects factor **ROI** ($F(2,4737) = 4515.938$, p < 0.001, $\eta_p^2 = 0.656$), no significant main effect of within-subjects factor **learning** ($F(1,4737) = 2.472$, p = 0.116, $\eta_p^2 = 0.001$), and a significant main effect of **task** ($F(2.085,9876.380) = 1000.788$, p < 0.001, $\eta_p^2 =$

0.174) on the VOI gradient values. The interactions, namely **learning*ROI** ($F(2,4737)$ = 3233.307, p < 0.001, η_p^2 = 0.577), **learning*task*ROI** ($F(3.26,7721.63)$ = 1126.755, p < 0.001, η_p^2 = 0.322), **task*ROI** ($F(4.17,9876.38)$ = 486.888, p < 0.001, η_p^2 = 0.171) and **learning*task** ($F(1.63,7721.63)$ = 873.567, p < 0.001, η_p^2 = 0.156) were all significant (Table 2 & 3).

These results align well with our hypothesis. Learning by itself does not change the mean gradient values; however, the task-condition does. Thus, each task-condition is characterised by a mean gradient value that reflects task-specific demands. Among the interactions, the greatest effect size was for learning*ROI. Thus, the mean gradient value for sub-ROIs were differentially shifted due to learning. The next biggest effect size was for learning*task*ROI. This indicates that the redistribution of gradient values for the ROIs with learning was task-dependent. Finally, task*ROI effect-size had the least effect-size among the interactions, but was significant, indicating that the sub-ROIs had mean gradient values which differed with the task-condition.

Table 2. Greenhouse-Geisser corrected tests of within-subjects effects

Source	Type III sum of squares	df	Mean square	F	Sig.	Partial eta squared
LEARNING	0.011	1.000	0.011	2.472	.116	.001
LEARNING*ROI	28.270	2.000	14.135	3233.307	.000	.577
Error (LEARNING)	20.709	4737.000	.004			
TASK	110.417	2.085	52.959	1000.788	.000	.174
TASK*ROI	107.437	4.170	25.765	486.888	.000	.171
Error (TASK)	522.632	9876.380	.053			
LEARNING*TASK	12.577	1.630	7.716	873.567	.000	.156
LEARNING*TASK* ROI	32.445	3.260	9.952	1126.755	.000	.322
Error (LEARNING*TASK)	68.202	7721.630	.009			

Table 3. Tests of between-subjects effects

Source	Type III sum of squares	df	Mean square	F	Sig.	Partial eta squared
INTERCEPT	3804.284	1	3804.284	5585.615	.000	.541
ROI	6151.483	2	3075.742	4515.938	.000	.656
Error	3226.304	4737	.681			

Discussions

Change in task-specific distribution of connectopic gradient values following learning

As the task in every condition is grounded in the same extrinsic functional demands before and after learning, we assume that a fixed value along the respective functional gradient corresponds to the same functional region in both the maps before and after learning. We hypothesise that the modes of the normalised gradient values give us information about the functionally important VOI clusters along the connectopy. The two extremes of the gradient topographically map onto the two regions which are maximally distinct from each other with respect to their task-functional connectivity with the rest of the brain.

A natural extrapolation is that the change in gradient value for each voxel (with learning) is a direct representation of a relative shift in functionality of the said voxel towards either functional pole. Moreover, if the difference between the gradient values of two voxels decreases after learning, it effectively signifies functional integration between the said-voxels due to learning. If the difference increases, it signifies functional segregation

To understand this, let us first take a look at the distribution of gradient values along the dominant connectopy obtained for the task conditions colour-perception (**CP**), position-response (**PR**), and face-perception (**FP**) both before and after learning (Fig. 6, 7 & 8). In Fig. 7, the left mode shifts further left, and the right mode shifts further right. This suggests large-scale segregation across the entire visual ROI. In Fig. 8 we observe three modes in the distribution. Considering new evidence for a distinct visual pathway specialised for social perception[11], we hypothesise that the middle mode maps onto regions specifically involved in face-perception, which intuitively, functionally integrate with the V1/V2 region following learning.
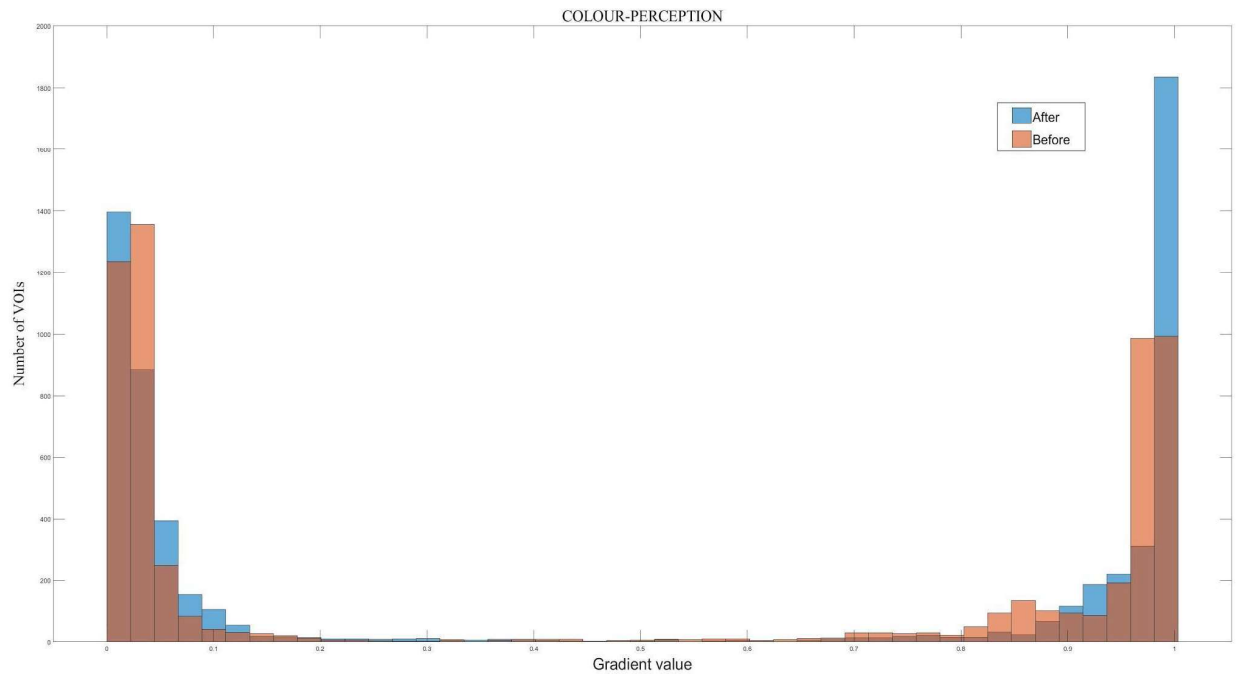
Figure 6. Distribution of gradient values for the CP task-condition, before and after learning. Note the sharper distribution close to gradient value 1 following learning. Figure generated in Matlab.
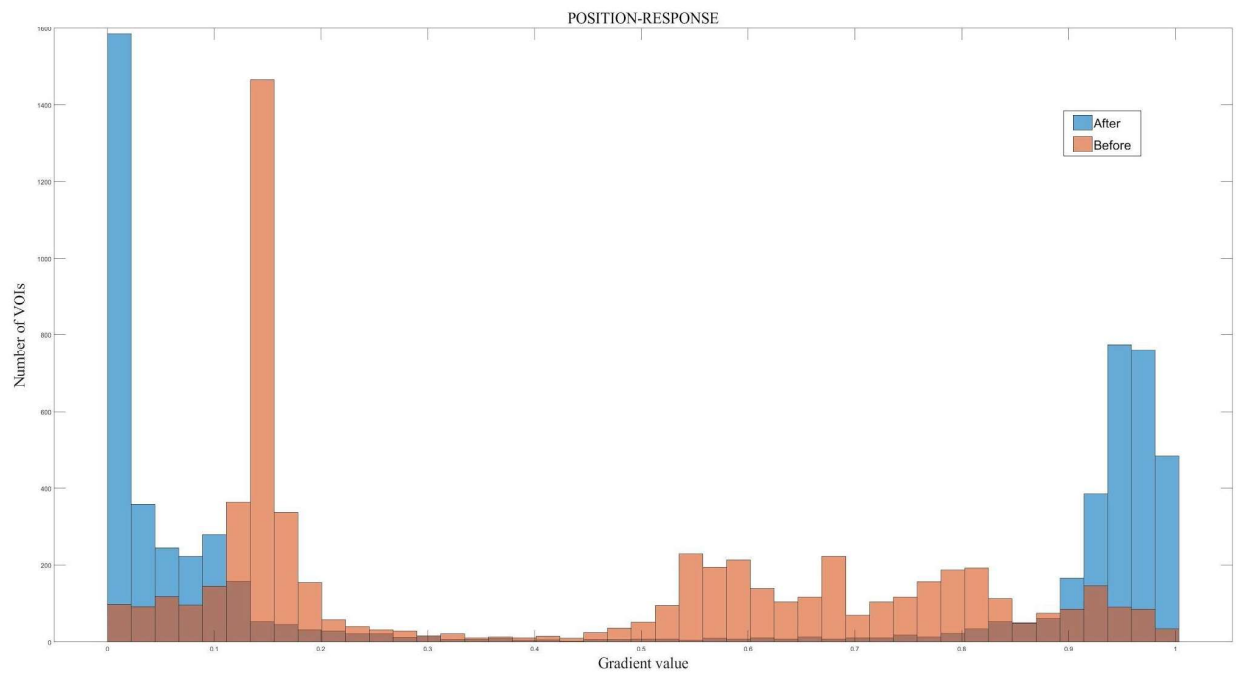

Figure 7. Distribution of gradient values for the PR task-condition, before and after learning. Note the segregation of the modes of the distribution towards the two extremes, following learning. Figure generated in Matlab.
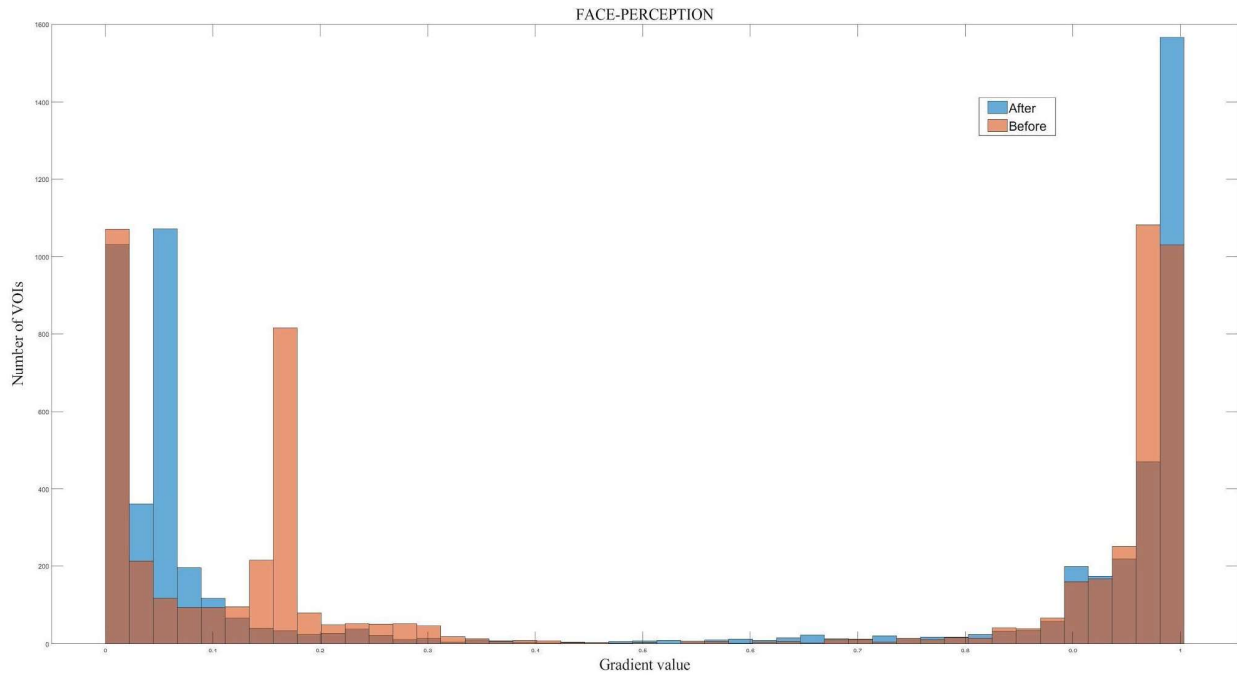
Figure 8. Distribution of gradient values for the FP task-condition, before and after learning. Note the trimodality of the distribution, as well as the segregation of the modes of the distribution towards the two extremes, with the middle-mode integrating strongly with the lower mode following learning. Figure generated in Matlab.

Visualisation of VOIs which drive the change in distribution of gradient values following learning

To visualise the VOIs which change their gradient value with learning and drive the change in gradient distribution, we construct the **dcmap** (cmap_after - cmap_before) for all task-conditions. Negative values mean the voxels have shifted towards the 0-end of the functional-connectopy, while positive values indicate the voxels have shifted towards the 1-end of the functional-connectopy. The idea is illustrated for **CP**, **PR** and **FP**conditions in Fig. 9, 10 and 11 respectively.
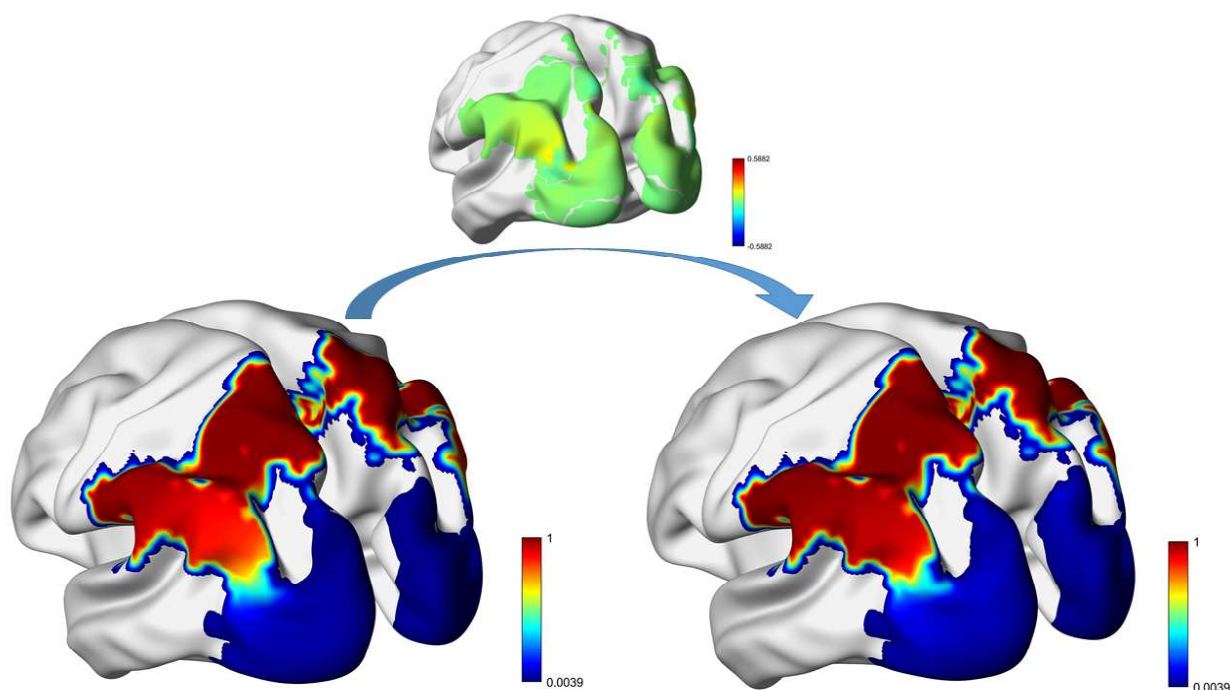

Figure 9. Connectopic map for CP condition before (left) and after (right) learning. The dcmap is above the arrow that depicts learning. Note, for example, the increase in gradient values in the angular gyrus, corresponding to the positive (yellow) dcmap values. Figure generated using BrainNet Viewer and Microsoft PowerPoint.
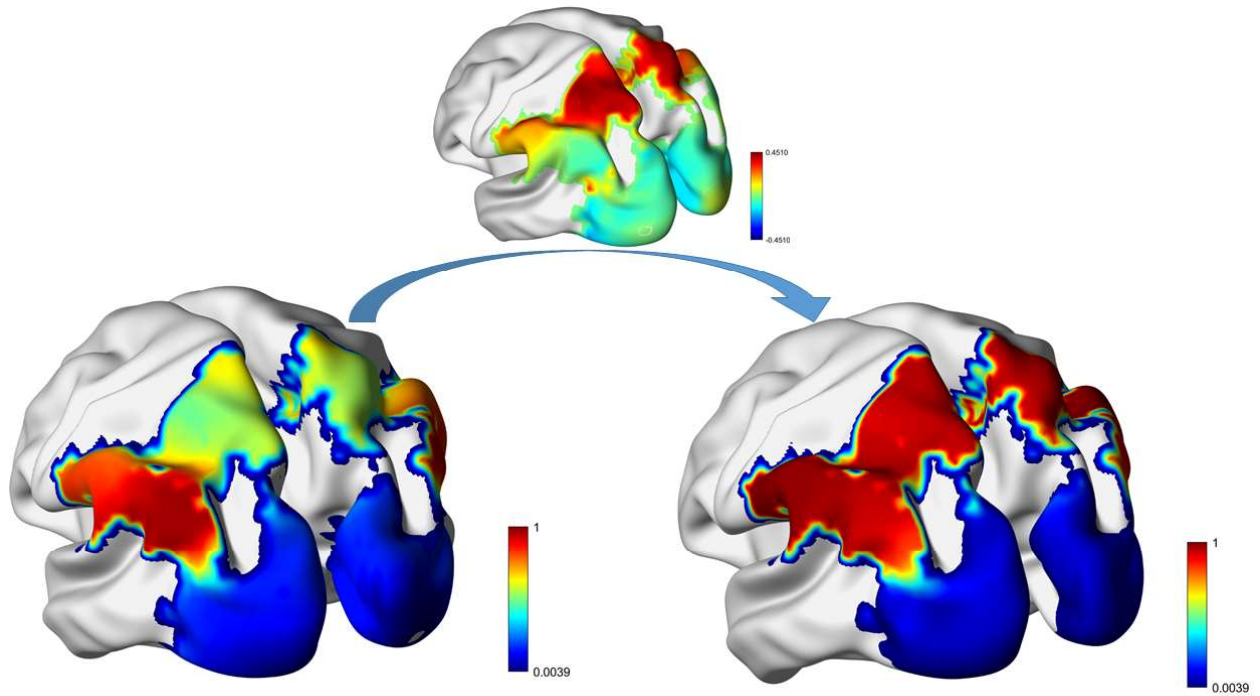
Figure 10. Connectopic map for PR condition before (left) and after (right) learning. The dcmap is above the arrow that depicts learning. Note, for example, the increase in gradient values in the superior and inferior parietal lobules, corresponding to the positive (orange-red) dcmap values. Figure generated using BrainNet Viewer and Microsoft PowerPoint.
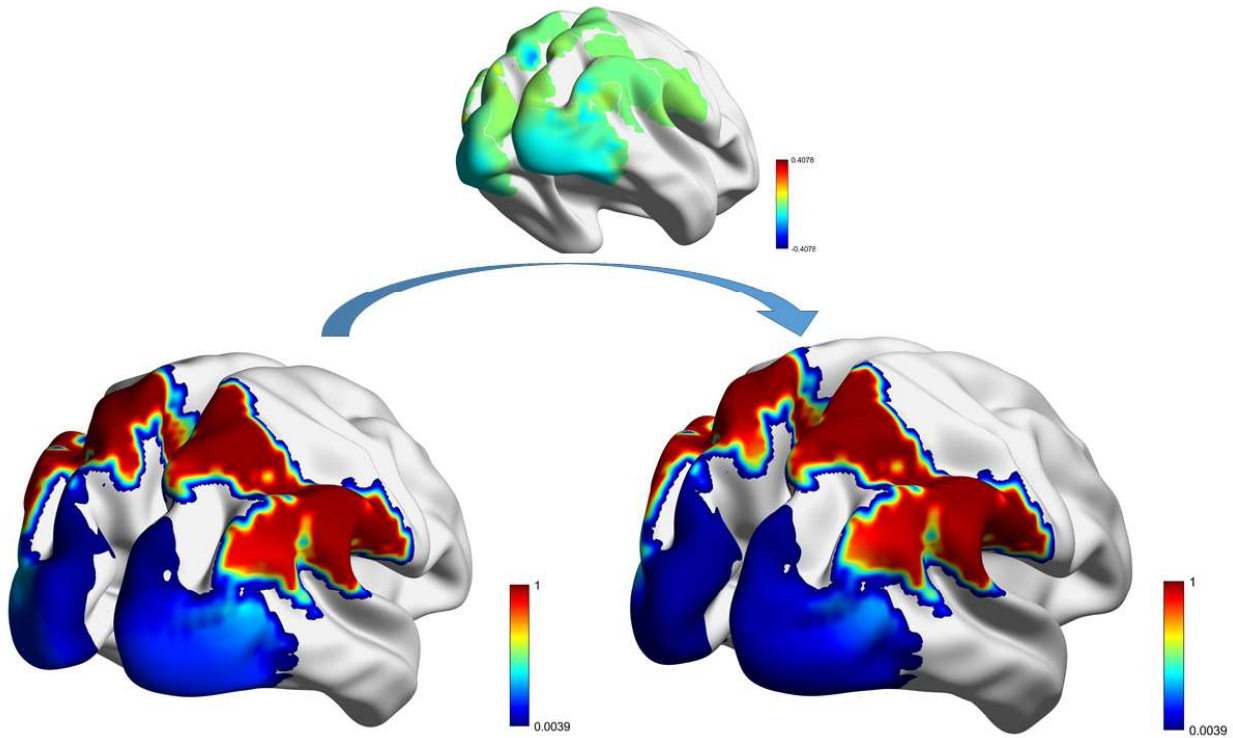
Figure 11. Connectopic map for FP condition before (left) and after (right) learning. The dcmap is above the arrow that depicts learning. Note the decrease in gradient values in the lingual and fusiform gyri, corresponding to the negative (turquoise) dcmap values. It seems like these are the regions involved in social perception, and this is supported by canonical knowledge in the field. Figure generated using BrainNet Viewer and Microsoft PowerPoint.

Visualisation of within and between-ROI integration/segregation at once

Another elegant way to visualise the distribution of gradient values sub-ROI-wise (the three sub-ROIs we are interested in are the *ventral stream*, *V1/V2 and dorsal stream)*, is illustrated in Fig. 12, 13 and 14 for the **CP**, **PR** and **FP** task-conditions respectively. Note that this figure gives us an idea of within-ROI integration. For example, in Fig. 11, strong within-dorsal-stream, within-V1/V2 and within-ventral-stream integration are evident from the band-like scatter of VOI gradient-values. The spread is greater along the x-direction (before learning) than along the y-direction (after learning) for all the three sub-ROIs.

Figure 12. For each voxel within the three ROIs, their gradient value after and before learning (CP tas-condition) are plotted on the y and x-axis respectively. Points above the plotted line are the ones whose gradient value has increased with learning and vice versa. Figure generated in Matlab.
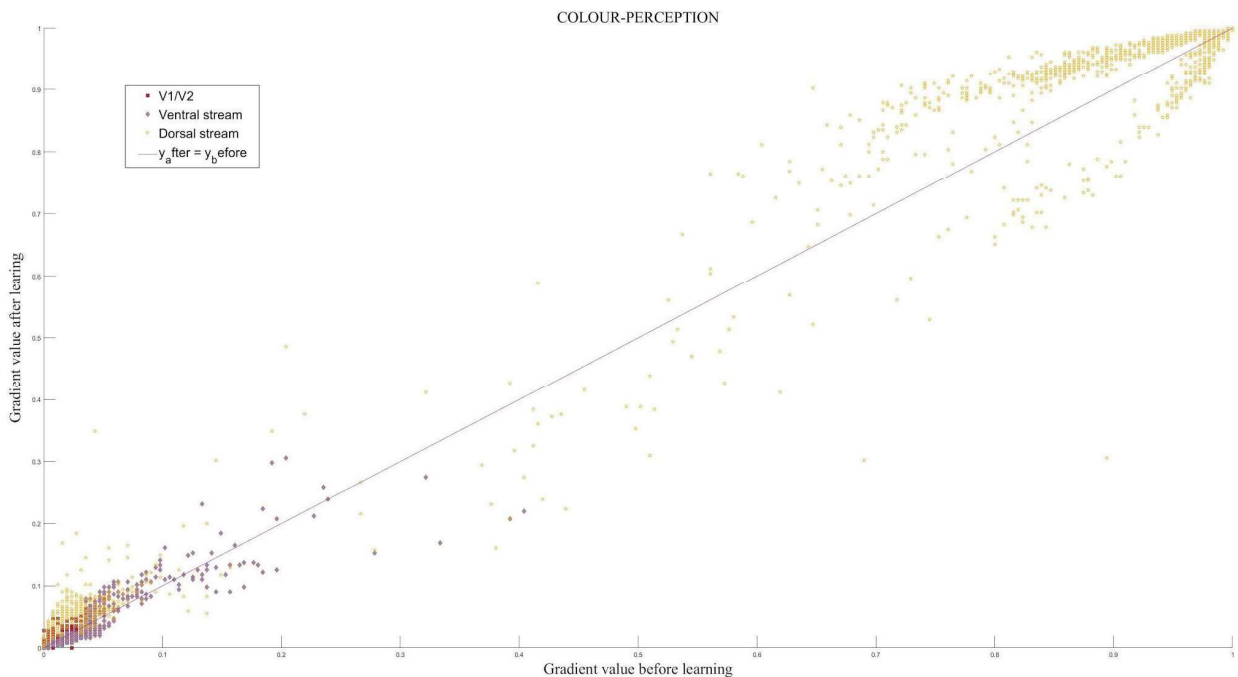
Figure 13. For each voxel within the three ROIs, their gradient value after and before learning (PR task-condition) are plotted on the y and x-axis respectively. Note how the dorsal stream VOIs had a wide distribution before learning, as opposed to a very narrow distribution close to 1 after learning. The distribution also narrows and moves closer to 0 for the ventral stream VOIs. Figure generated in Matlab.
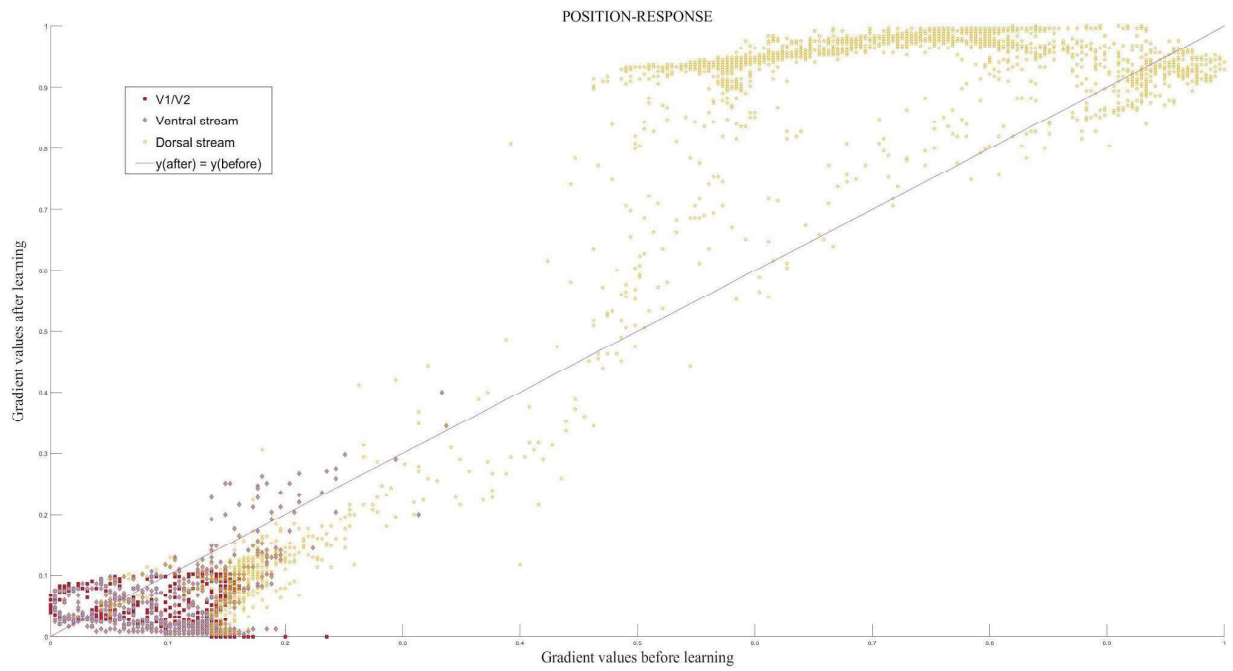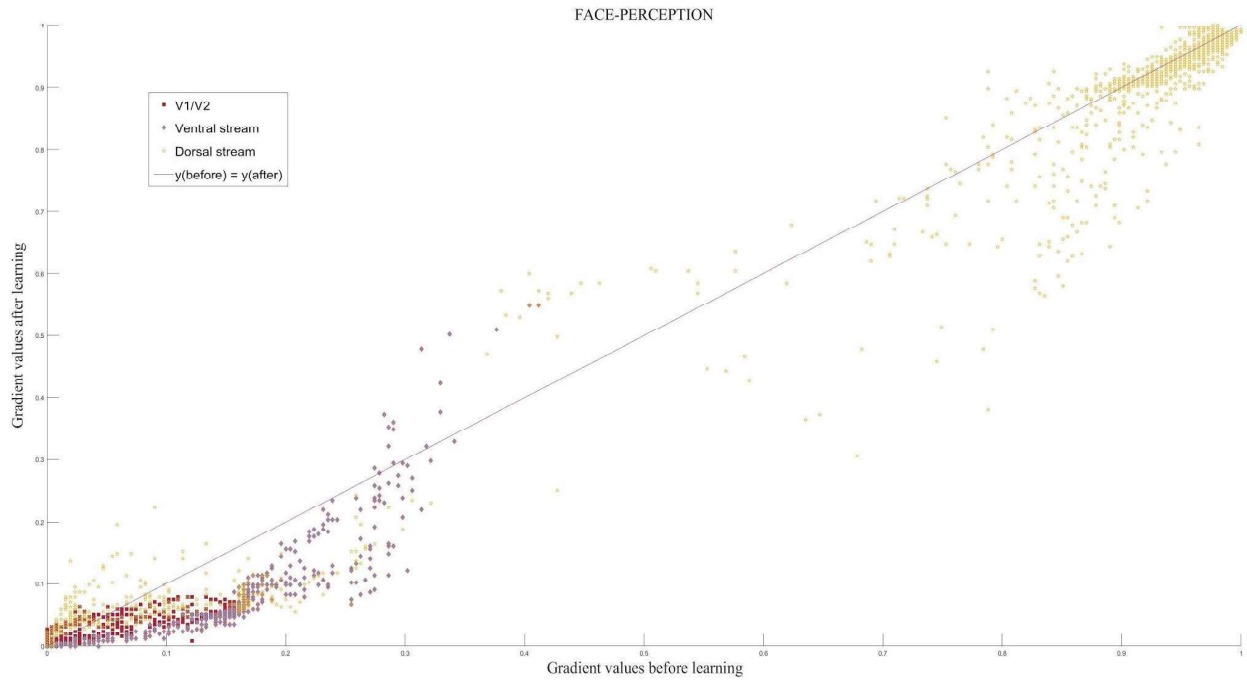
Figure 14. For each voxel within the three ROIs, their gradient value after and before learning (FP task-condition) are plotted on the y and x-axis respectively. Note how most of the VOIs have moved closer to zero following learning. The V1/V2 and ventral stream ROIs seem to have narrowed down their distribution too, due to learning. Figure generated in Matlab.

Task-specific changes in marginal means of ROI-wise gradient values with learning

Finally, to discern between-ROI integration/segregation with learning across different tasks, we look at the line-charts of marginal means (ROI-wise centers-of-function), with each plot representing a separate task-condition, and the two lines per-plot representing the connectopic profile before and after learning. In all figures, ROIs are grouped as: 1 - Ventral stream, 2 - V1/V2, and 3 - Dorsal stream. Learning is levelled as: 1 - Before learning and 2 - After learning. Error bars represent +/- 2 Standard Error.
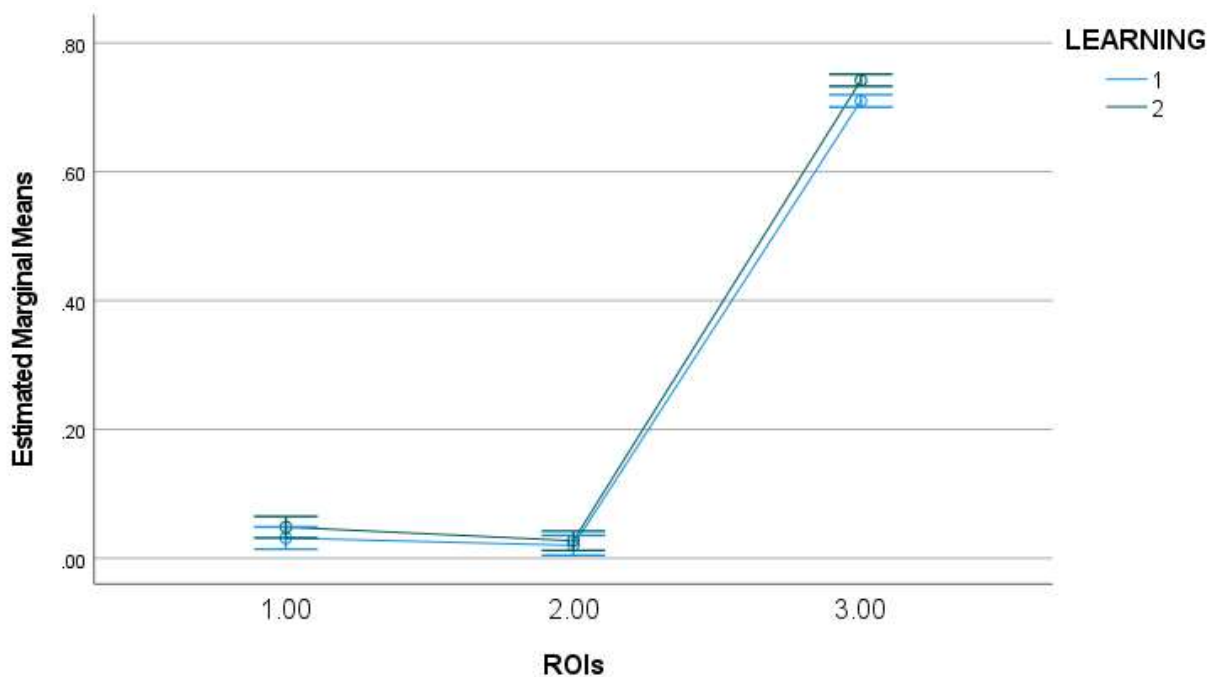
Figure 15. CP task-condition. We see no significant shift of V1/V2 values with learning, while both ventral stream and dorsal stream values increase. Thus, there takes place functional segregation between the ventral stream and V1/V2, as well as between the ventral stream and dorsal stream. Figure generated in IBM SPSS.
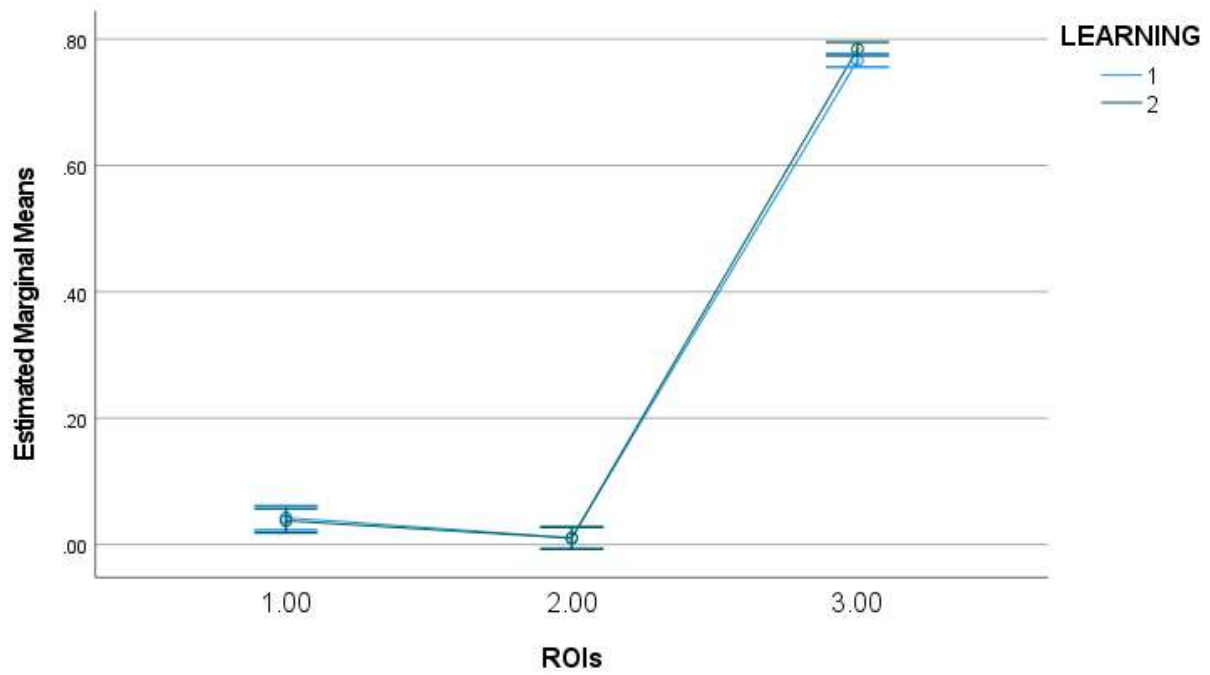
Figure 16. CR task condition. There only seems to be slight segregation between V1/V2 and dorsal stream, as well as small segregation between the ventral stream and V1/V2. Figure generated in IBM SPSS.
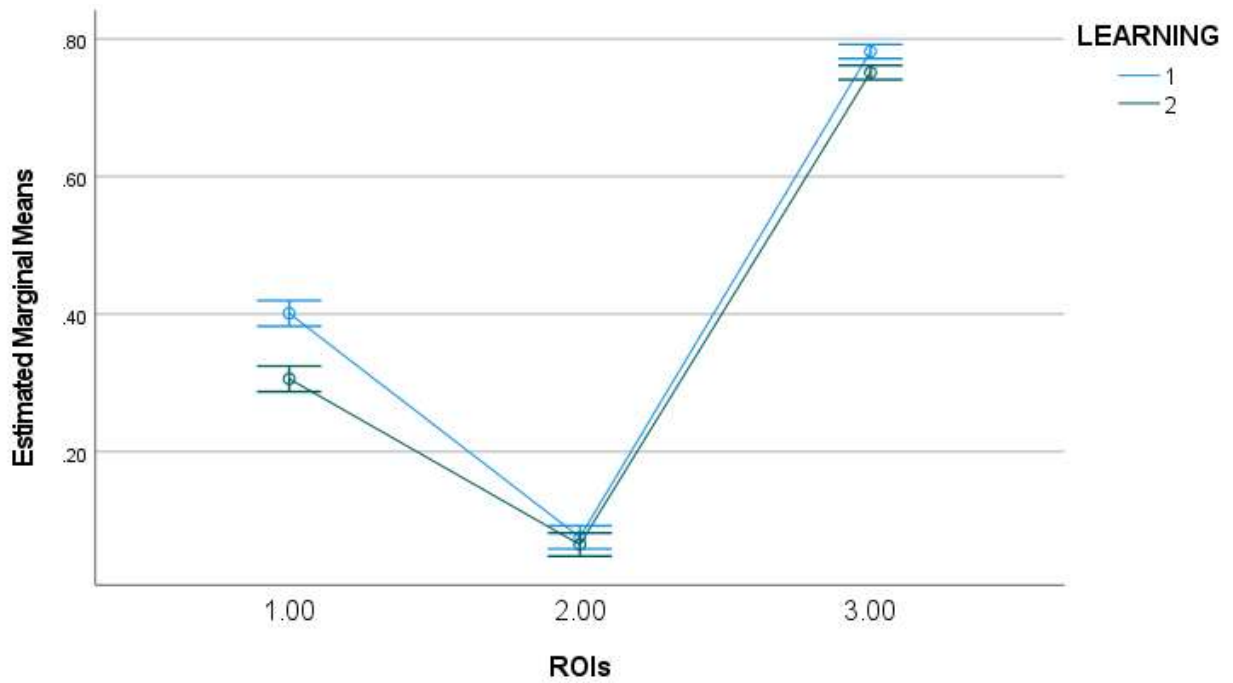
Figure 17. PP task condition. There happens to be strong integration between the ventral stream and V1/V2, and a relatively weaker integration between V1/V2 and the dorsal stream. Overall, there is also segregation apparent between the ventral stream and dorsal stream. Figure generated in IBM SPSS.
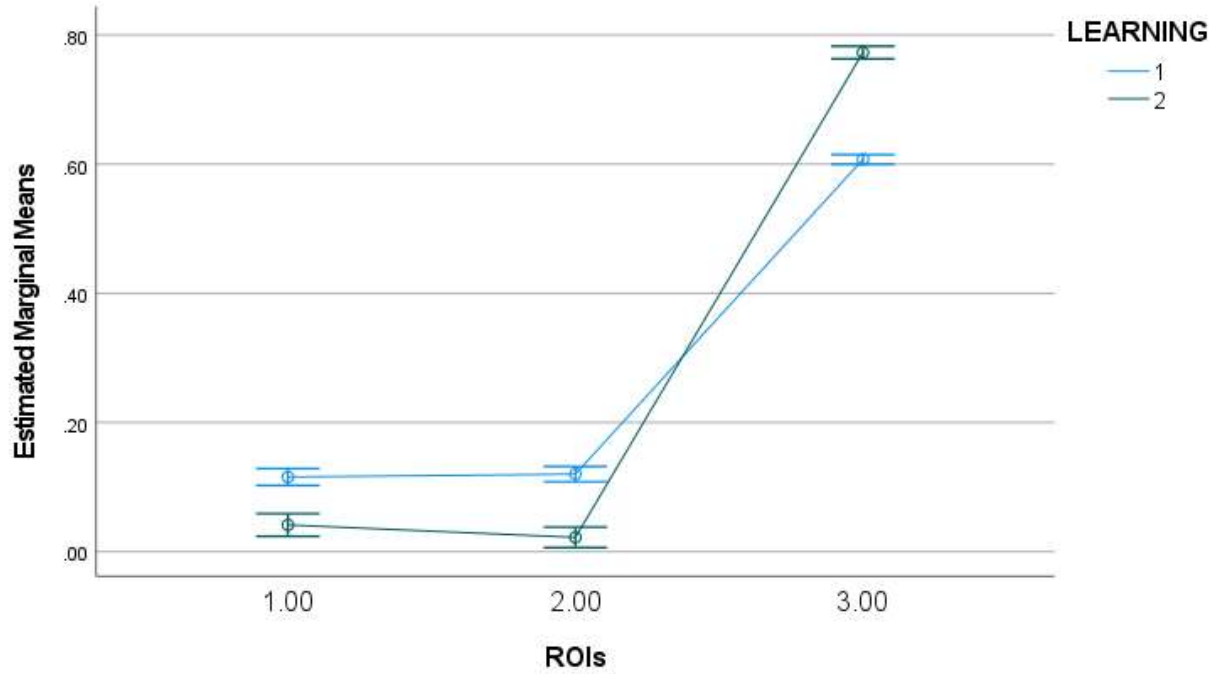
Figure 18. PR task condition. There is slight segregation between the ventral stream and V1/V2, and strong segregation between both ventral stream and dorsal stream, as well as between V1/V2 and dorsal stream. Figure generated in IBM SPSS.

Figure 19. FP task condition. There happens strong integration between the ventral stream and V1/V2, strong segregation between the ventral stream and dorsal stream, and relatively weaker segregation between V1/V2 and dorsal stream. Figure generated in IBM SPSS.

Figure 20. FR task condition. There happens, with learning, a weak functional integration between the ventral stream and V1/V2, and strong segregation between both ventral stream and dorsal stream, as well as between V1/V2 and dorsal stream. Figure generated in IBM SPSS.
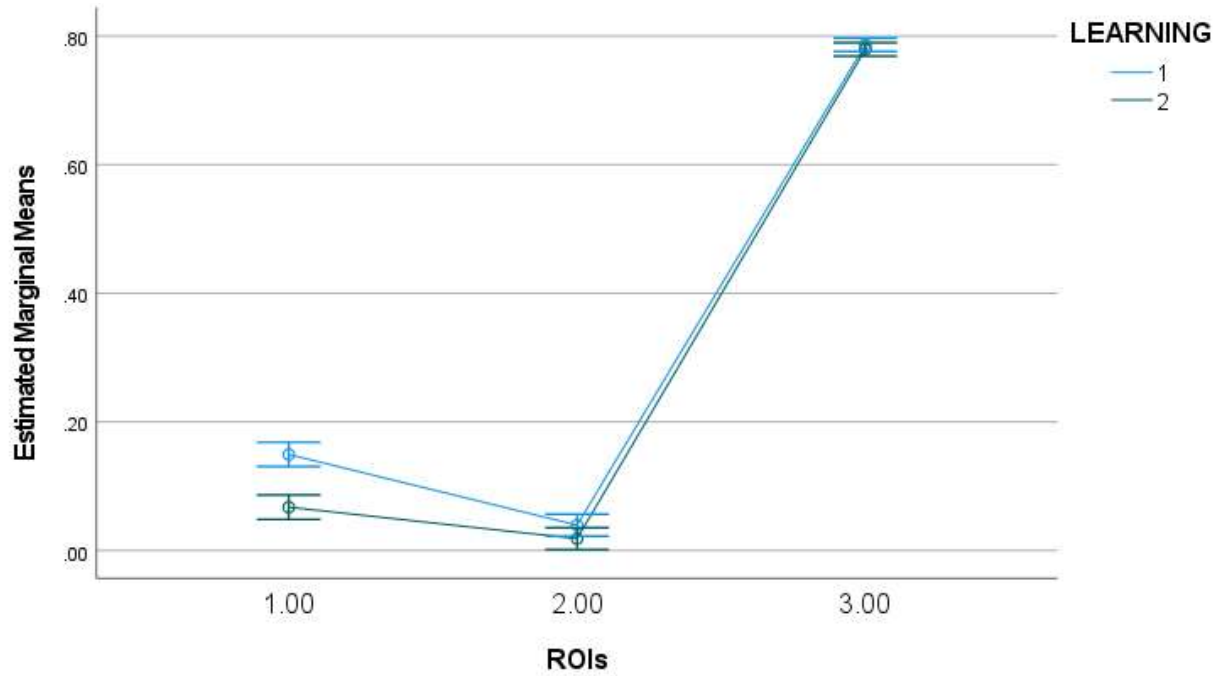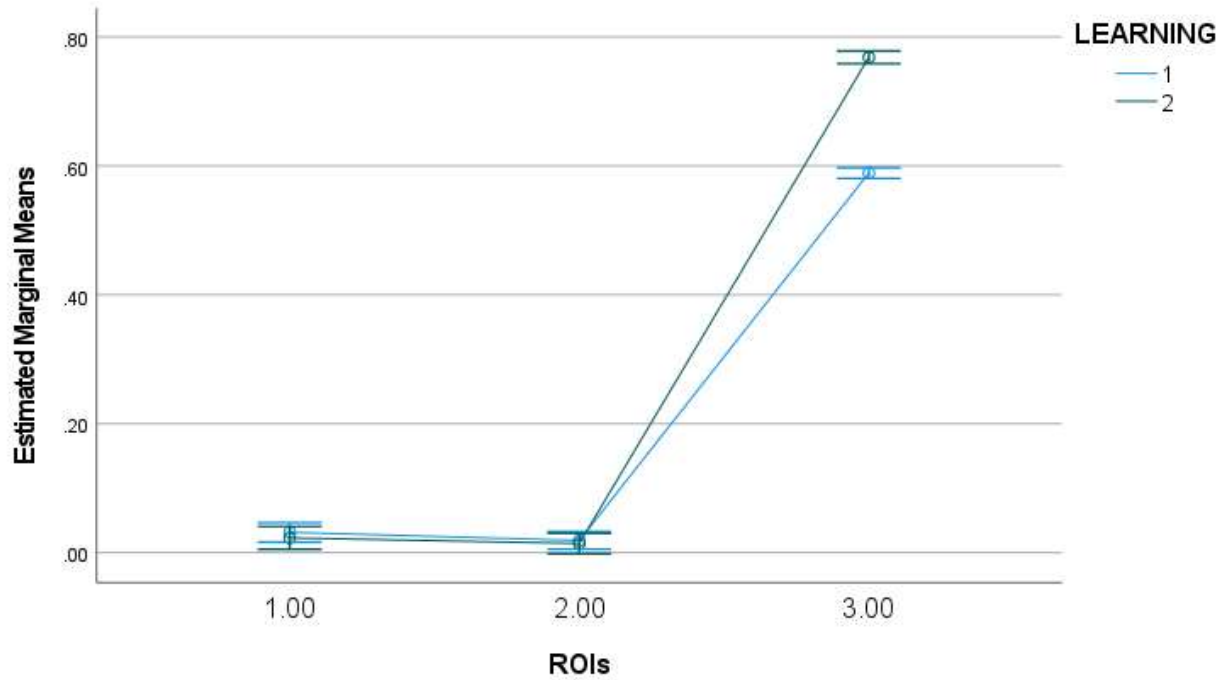
Conclusion

One of the most important ideas in network neuroscience is learning, and one of the key questions is- how do we quantify it? There are many advantages of being able to put our finger on the neural-network correlates of task-learning. For example, the development of personalised biomarkers can track effective learning in patients with somatosensory or socio-cognitive impairments.

In this study, we identify the functional spectrum of the visual-processing system along its dominant mode of topographic connectivity. Moreover, we use this approach to analyse functional integration, segregation, as well as overall functional shifts of brain regions with learning. We adapt the data-driven pipeline developed by Haak et al. that was used with resting-fMRI, and perform our analysis on task-fMRI recordings across six different kinds of tasks. We also find nascent evidence to support the idea of a third visual pathway involved in social perception.

Much work however remains to be done in order to establish connectopic mapping and connectopic parcellation as a frontier tool to probe task-specific learning. Two major directions for future work are:

a) Connectopic mapping on individual subjects for all the response-task conditions. After doing this, we aim to try and use the intra-class correlation between individual and group-average maps to predict their behavioural scores, as well as relative improvement of task-performance for each participant.

b) Parcellation of the ROI by binning the gradient values into, say, 45 bins, followed by principal component analysis on the pooled BOLD-activation data-matrix (on the binned gradient map), with each participant in each task condition along one row, and matrix values representing average BOLD signal from all voxels within that gradient-value bin, for the said participant, performing said task. We will try to identify if there are independent spatial components within our ROI that contribute more heavily to the activation map during specific conditions of interest. This will be done by examining the PCA-loading of obtained

principal components. We shall do this separately for before and after learning, to find out which components increase (or decrease) in their activity with learning, and in which task-conditions.

References

1. Jbabdi, S., Sotiropoulos, S. N. & Behrens, T. E. The topographic connectome. *Current Opinion in Neurobiology* vol. 23 207–215 (2013).

2. Heinzle, J., Kahnt, T. & Haynes, J.-D. Topographically specific functional connectivity between visual field maps in the human brain. *Neuroimage* **56**, 1426–1436 (2011).

3. Greenberg, A. S. *et al.* Visuotopic Cortical Connectivity Underlying Attention Revealed with White-Matter Tractography. *Journal of Neuroscience* vol. 32 2773–2782 (2012).

4. Thivierge, J.-P. & Marcus, G. F. The topographic brain: from neural connectivity to cognition. *Trends in Neurosciences* vol. 30 251–259 (2007).

5. Tinsley, C. J. Using topographic networks to build a representation of consciousness. *Biosystems.* **92**, 29–41 (2008).

6. Mishkin, M., Ungerleider, L. G. & Macko, K. A. Object vision and spatial vision: two cortical pathways. *Trends in Neurosciences* vol. 6 414–417 (1983).

7. Goodale, M. A. & David Milner, A. Separate visual pathways for perception and action. *Trends in Neurosciences* vol. 15 20–25 (1992).

8. Ray, D., Hajare, N., Roy, D. & Banerjee, A. Large-scale Functional Integration, Rather than Functional Dissociation along Dorsal and Ventral Streams, Underlies Visual Perception and Action. *J. Cogn. Neurosci.* **32**,

847–861 (2020).

9.	Haak, K. V., Marquand, A. F. & Beckmann, C. F. Connectopic mapping with resting-state fMRI. *Neuroimage* **170**, 83–94 (2018).

10.	Weinberger, Kilian Q., and Lawrence K. Saul. Unsupervised learning of image manifolds by semidefinite programming. *International journal of computer vision* **70.1**, 77-90 (2006):

11.	Pitcher, D. & Ungerleider, L. G. Evidence for a Third Visual Pathway Specialized for Social Perception. *Trends Cogn. Sci.* **25**, 100–110 (2021).

APPENDIX I

Sl. No.	Checkpoint	Yes/No	Percent/word-count/consistent/number
1.	Plagiarism	Y	Done
2.	Grammar by Grammarly	Y	Done
3.	Spelling check	Y	Done
4.	Reference format	Y	Nature
5.	Reference font	Y	Times New Roman
6.	Number of references	Y	11
7.	Legends in figures	Y	Added
8.	Legends in tables	Y	Added
9.	Length of abstract	Y	140
10.	Length of Introduction	Y	662
11.	Length of Materials and Methods	Y	1712
12.	Length of Results	Y	597
13.	Length of Discussion	Y	1196
14.	Length of Conclusion	Y	344
15.	Length of References	Y	2 pages
16.	Length of Appendices	Y	2 pages
17.	Number of figures	Y	20
18.	Figure permissions	Y	None required
18.	Number of tables	Y	3
19.	MS thesis format	Y	PDF
20.	MS thesis font	Y	Times New Roman
21.	Correct numbering of contents	Y	Checked
22.	Page numbers	Y	35
23.	Figures and tables in the correct order	Y	Checked

APPENDIX   II

IISERB

Yudhajit Ain 16231 <yudhajit16@iiserb.ac.in>

Thesis comments

Arpan Banerjee <arpan@nbrc.ac.in>
To: Yudhajit Ain 16231 <yudhajit16@iiserb.ac.in>

Thu, Apr 22, 2021 at 6:23 PM

Dear Yudhajit,

I have put my edits in the thesis. Overall it reads nice! You can treat this as final from my side unless you make changes to declaration page and comments regarding ethics in Methods. Please check for weird characters, most likely coming from your copy paste from pdf.

Please cite our Bioarxiv article as well - which was published with the appropriate creative commons license that allows you to use for academic purpose while referring to the Fig 2. In any case as the senior author of that paper and custodian of this data set, you certainly have my approval for use of the Figure.

Best wishes

Arpan

--
This email has been checked for viruses by AVG.
https://www.avg.com

MS thesis_AB.docx
4278K

APPENDIX III

IISERB   Yudhajit Ain 16231 <yudhajit16@iiserb.ac.in>

Proposed modification of copyright declaration for MS thesis

Dean, Academic Affairs <doaa@iiserb.ac.in>   Sun, Apr 25, 2021 at 8:27 AM
To: Yudhajit Ain 16231 <yudhajit16@iiserb.ac.in>
Cc: "Head, Department of Biological Sciences" <hod_bio@iiserb.ac.in>

Dear Yudhajit,

My apologies for late reply. Yes, the disclaimers are fine with me. Please go ahead.

Snigdha.

On Fri, 23 Apr 2021, 11:56 Yudhajit Ain 16231, <yudhajit16@iiserb.ac.in> wrote:
Dear ma'am and sir,

Please find attached the copyright disclaimer from both the official thesis format of IISERB and the one that Dr. Arpan proposes.

Kindly note that in neither of them do I, as a signatory, directly ascribe the copyright of the thesis document to either institute. In the proposed modification however, I mention (in an open-access fashion) that I am fine with any researcher using the intellectual contents of my thesis to progress research.

I hope to clarify this confusion soon, and will rely on both of your sage advice on the same.

Yours faithfully,

Yudhajit.

Indian Institute of Science Education and Research, Bhopal.
email: yudhajitain@gmail.com
       yudhajit16@iiserb.ac.in
phone: +91 9593803376

MS_yudhajit.pdf

1 Dipanjan Ray, Nilambari Hajare, Dipanjan Roy, Arpan Banerjee. "Large-scale functional integration, rather than functional dissociation along dorsal and ventral streams, underlies visual perception and action", Cold Spring Harbor Laboratory, 2020
Publication

1%

2 Carol Boon Peng Loy-Ee, Patricia Mui Hoon Ng. "Dental Health Curriculum for Pre-Schoolers With Robot Application Intervention", International Journal of Curriculum Development and Learning Measurement, 2021
Publication

1%

3 Chunshui Yu. "Altered functional connectivity of primary visual cortex in early blindness", Human Brain Mapping, 05/2008
Publication

<1%

4 Jahangir Mardali, Masood Siyyari, Xiaofei Lu. "English teachers' beliefs and practices in

<1%

teaching vocabulary: The case of teaching experience", Cogent Education, 2019
Publication

5   Mervyn Yeo, Eugene Tham, Lijun Jiang. "Mind-focus onset of the physically challenged", 2012 7th IEEE Conference on Industrial Electronics and Applications (ICIEA), 2012
Publication
<1%

6   Ton J. Cleophas, Aeilko H. Zwinderman. "SPSS for Starters and 2nd Levelers", Springer Science and Business Media LLC, 2016
Publication
<1%

7   Nave, R.D.. "Brain white matter damage in SCA1 and SCA2. An in vivo study using voxel-based morphometry, histogram analysis of mean diffusivity and tract-based spatial statistics", Neuroimage, 20081015
Publication
<1%